View Article Online
View Journal

Dalton Transactions

An international journal of inorganic chemistry

Accepted Manuscript

This article can be cited before page numbers have been issued, to do this please use: S. Ferrari, E. Karaca and D. Errandonea, *Dalton Trans.*, 2026, DOI: 10.1039/D6DT00593D.

ROYAL SOCIETY OF CHEMISTRY

rsc.li/dalton

View Article Online
DOI: 10.1039/D6DT00593D

Journal Name

ARTICLE TYPE

Cite this: DOI: 00.0000/xxxxxxxxxx

Systematic first-principles study of pressure-induced phase transitions and lattice properties in lanthanide monosulfides

Sergio Ferrari[a,b], Ertuğrul Karaca[c,d] and Daniel Errandonea[e,*]

Received Date
Accepted Date

DOI: 00.0000/xxxxxxxxxx

We present a systematic *ab-initio* investigation of the structural, elastic, and vibrational properties of lanthanide monosulfides (LnS, Ln = La–Lu) under pressure using density-functional theory within the plane-wave pseudopotential framework implemented in Quantum ESPRESSO. Total-energy calculations combined with Birch–Murnaghan equations of state reveal that all compounds are thermodynamically stable in the NaCl-type (B1) structure at ambient conditions and undergo a pressure-induced phase transition to the CsCl-type (B2) structure upon compression. The calculated transition pressures increase monotonically along the lanthanide series, from 22 GPa in LaS to 66 GPa in LuS, reflecting the contraction of the lanthanides. A notable exception is YbS, which exhibits an anomalously low bulk modulus and transition pressure because of the stability of the divalent Yb electronic configuration at ambient pressure. Elastic constant calculations confirm the mechanical stability of both B1 and B2 phases and reveal systematic trends in ductility and stiffness throughout the series. Phonon dispersion relations show that both phases are dynamically stable, with the B2 structure exhibiting softer lattice vibrations and enhanced compressibility relative to the B1 phase. The combined analysis of structural, elastic, and vibrational properties provides a comprehensive description of the high-pressure behavior of lanthanide monosulfides and offers predictive guidance for future experimental studies.

1 Introduction

Lanthanide monosulfides (LnS, Ln = La–Lu) constitute an important class of rare-earth chalcogenides that exhibit a wide range of physical properties arising from the interplay between localized 4f electrons and the crystal lattice. These compounds have attracted considerable interest due to their potential applications in areas such as solar-energy conversion, optical materials, pigments, and cold-cathode technologies[1]. In addition, their electronic structures give rise to a variety of intriguing phenomena including complex magnetic ordering, pressure-induced insulator–metal transitions, valence fluctuations, and unusual Fermi-surface characteristics[2].

Under ambient conditions, lanthanide monosulfides crystallize in the NaCl-type (B1) structure with space group $Fm\bar{3}m$[3]. In this structure, each lanthanide atom is octahedrally coordinated by six sulfur atoms, forming a highly symmetric ionic lattice. These compounds are particularly interesting from a materials perspective because they can provide low or even negative electron affinity when deposited on certain semiconductor substrates, offering advantages over alkali metals in cold-cathode applications[1]. Several synthesis methods have been reported, including electrolytic reduction of higher sulfides in fused salt media, direct reaction between elemental lanthanides and sulfur, reduction of Ln_2S_3 powders with metallic lanthanides, and chemical vapor deposition techniques[4–6].

Despite the technological relevance of lanthanide monosulfides, their structural and high-pressure (HP) behavior remains relatively underexplored compared to other rare-earth compounds[7]. Experimental and theoretical investigations have primarily focused on individual members of the lanthanide series, often comparing them with related monopnictides and monochalcogenides[8–13]. However, there is a lack of a unified understanding of systematic trends across the entire lanthanide family. High-pressure studies are particularly valuable as compression can significantly alter bonding environments, electronic

[a] *Departamento Física Nuclear y Tecnología de Recubrimientos, CNEA, Centro Atómico Constituyentes, Av. Gral. Paz 1499, 1650 San Martín, Argentina*
[b] *Consejo Nacional de Ciencia y Tecnología, Argentina*
[c] *Sakarya University, Faculty of Sciences, Department of Physics, 54050, Sakarya, Turkey; E-mail: ertugrulkaraca@sakarya.edu.tr*
[d] *School of Physics, Engineering & Technology, University of York, York YO10 5DD, United Kingdom; E-mail: ertugrul.karaca@york.ac.uk*
[e] *Departamento de Fisica Aplicada-ICMUV, MALTA Consolider Team, Universitat de Valencia Av. Dr. Moliner 50, 46100 Burjassot (Valencia), Spain; E-mail: daniel.errandonea@uv.es*
[*] Corresponding author

View Article Online
DOI: 10.1039/D6DT00593D

configurations, and lattice dynamics. These changes often induce structural phase transitions and modify physical properties [14,15].

Previous investigations have shown that lanthanum monosulfide (LaS) [8,13], praseodymium monosulfide (PrS) [9], samarium monosulfide (SmS) [10], and europium monosulfide (EuS) [11,12] undergo a pressure-induced structural transformation from the B1 to the B2 (CsCl-type) structure. This behavior reflects the general tendency of ionic compounds with the NaCl structure to adopt higher-coordination phases under compression. In the case of EuS, however, there is no consensus regarding the transition pressure, with reported values ranging from 11.6 to 21.5 GPa [11,12]. Additionally, a theoretical study predicted a similar B1→B2 transition in ytterbium monosulfide (YbS), although the estimated transition pressure (9.4 GPa) [12] is significantly lower than those reported for LaS (24.9 GPa) [8] and PrS (22 GPa) [9]. The high-pressure structural behavior of the remaining lanthanide monosulfides has not yet been systematically investigated. Furthermore, previous calculations have employed a variety of computational approaches, including the linear muffin-tin orbital (LMTO) method [8], the self-interaction-corrected (SIC) local spin density (LSD) approximation [9], and tight-binding calculations assuming a three body interaction [12]. The use of different methodologies across these studies hinders direct comparison of the results.

This situation contrasts with that of lanthanide monoxides, for which a recent theoretical work has examined the complete series using a consistent computational framework, revealing clear systematic trends governed by the lanthanide contraction [7]. The progressive filling of localized 4f orbitals across the lanthanide series leads to a gradual reduction in ionic radii, which in turn influences structural stability, compressibility, and phase transition pressures. Extending such systematic investigations to lanthanide monosulfides is therefore essential for developing a comprehensive understanding of how lanthanide contraction and electronic configuration affect the structural and vibrational properties of rare-earth chalcogenides.

First-principles calculations based on density-functional theory (DFT) provide a powerful framework for addressing these questions [16,17]. DFT methods allow reliable predictions of structural stability, elastic properties, and lattice dynamics while offering atomistic insight into the mechanisms governing phase transitions under pressure. In systems containing lanthanide elements, these calculations are particularly valuable because they enable systematic comparisons across the entire series while overcoming the experimental challenges associated with HP measurements.

In this work, we present a comprehensive first-principles investigation of the structural, elastic, and vibrational properties of lanthanide monosulfides (LnS, Ln = La–Lu) under pressure. By examining the complete lanthanide series within a unified computational framework, we establish systematic trends associated with the lanthanide contraction and identify anomalies related to specific electronic configurations. In particular, we determine equilibrium structural parameters, bulk moduli, and pressure-induced B1→B2 transition pressures, and analyze the mechanical stability of both phases through elastic-constant calculations. Furthermore, phonon dispersion relations are computed to evaluate the dynamical stability of the structures and to elucidate the evolution of lattice vibrations under compression.

The results provide a coherent picture of the high-pressure behavior of lanthanide monosulfides and reveal clear correlations between structural stability, elastic response, and lattice dynamics across the series. In addition, the calculations highlight the distinctive behavior of YbS, whose anomalous properties originate from the stability of the divalent ytterbium electronic configuration. These findings offer predictive insights into the structural properties of lanthanide sulfides and provide a useful reference for future experimental investigations of rare-earth chalcogenides under extreme conditions.

2 Method

The structural and HP properties of lanthanide monosulfides were investigated by means of *ab initio* calculations performed within Density Functional Theory (DFT), using the pseudopotential–plane-wave approach as implemented in the Quantum ESPRESSO package [18]. Calculations were performed at 0 K temperature. Ionic cores were described by ultrasoft pseudopotentials taken from the Standard Solid State Pseudopotentials (SSSP) library. During the generation of pseudopotentials, for sulfur atoms the $3s^2$ and $3p^4$ electrons were explicitly treated as valence electrons, while for lanthanide atoms all but one of the f electrons were frozen in the core. This approximation may slightly affect the detailed electronic structure of compounds, but is expected to have only a minor influence on equilibrium structural properties and relative phase stability [7]. Therefore, it is adequate to capture the systematic structural and vibrational trends emphasized in this work. However, although several lanthanide monosulfides exhibit magnetic ordering at low temperature [1], spin polarization is neglected because structural and vibrational properties are governed mainly by bonding and ionic size effects. Previous first-principles studies [13] indicate that magnetism has only a minor influence on equilibrium structures and relative phase stabilities.

The electronic wave functions were expanded in a plane-wave basis set with a kinetic-energy cutoff of 170 Ry, while a cutoff of 1360 Ry was employed for the charge density and potential. Brillouin-zone integrations were carried out using a 10×10×10 Monkhorst–Pack k-point mesh. These numerical parameters were selected on the basis of convergence tests to ensure the accuracy of the calculated total energies.

For each lanthanide monosulfide, total energies were computed for a set of different unit-cell volumes, equivalently generated by varying the cubic lattice parameter. This procedure yielded energy–volume data sets for the candidate crystal structures considered here. The resulting energy–volume curves were subsequently fitted using a Birch–Murnaghan equation of state (EOS) [19], from which the equilibrium lattice constant, equilibrium energy, bulk modulus, and its pressure derivative were extracted.

Once the equation-of-state parameters were obtained, the pressure dependence of the total energy was used to construct the enthalpy H according to:

$$H(p) = E(p) + p.V(p)$$

View Article Online
DOI: 10.1039/D6DT00593D

where the volume as a function of pressure was determined self-consistently from the same Birch–Murnaghan formalism using the fitted EOS. The enthalpy–pressure relations were then used to analyze the relative thermodynamic stability of the different phases and to identify pressure-induced structural phase transitions.

The HP behavior was examined considering the cubic structure reported in the literature for lanthanide monosulfides, namely B1, and also the cubic B2 structure. Only the B1 and B2 phases were considered because the $B1 \rightarrow B2$ transition is a generic and widely observed pressure-induced transformation in compounds adopting the NaCl-type structure, driven by the stabilization of a higher-coordination phase under compression[7]. This behavior is well established in related ionic systems, making B2 the most plausible HP candidate phase for lanthanide monosulfides. The structure B1 is described by the space group $Fm\bar{3}m$, with the lanthanide atom occupying the Wyckoff position $4a$ (0, 0, 0) and the sulfur atom located in the position $4b$ (1/2, 1/2, 1/2). The structure B2 belongs to space group $Pm\bar{3}m$, with the lanthanide atom at the $1a$ site (0, 0, 0) and sulfur at the $1b$ site (1/2, 1/2, 1/2).

The elastic properties of the studied materials were also analyzed. The elastic constants were determined using the strain-stress method, in which a set of finite deformations is applied to the equilibrium crystal structure, and the resulting stress tensors are evaluated. This method allows for an accurate determination of the independent elastic constants within the harmonic approximation. The calculations were performed as implemented in the thermo_pw code[20]. The elastic constants obtained were then used to determine the mechanical stability and elastic behavior of the compounds. The linear-response method was used to calculate the lattice dynamics of the compounds studied. A grid of of $32 \times 32 \times 32$ k points was chosen for Brillouin-zone (BZ) integrations. We calculated 29 dynamical matrices by symmetry for a $8 \times 8 \times 8$ q-point mesh in the irreducible BZ, which were Fourier-transformed to determine force constants. The constants were later used to produce the phonon dispersion curves and the phonon density of states for the compounds.

3 Results and Discussions

3.1 Crystal structure

By optimizing the crystal structure through total-energy minimization, we determined the equilibrium lattice parameter of each LnS compound at 0 GPa (a_0). Fitting the pressure-energy relationship to the Birch-Murnaghan EOS[19] yielded the bulk modulus at 0 GPa (K_0) and its pressure derivative (K_0'). Figure 1(a) shows an example of the results for LaS in the B1 structure. The calculated values for all compounds investigated here are summarized in Table 1.

As shown in Figure 2(a) and Table 1, the calculated equilibrium lattice parameters exhibit a clear and systematic decrease along the La–Lu series, reflecting the well-known lanthanide contraction. This trend is consistently reproduced for most studied compounds, confirming the internal consistency and reliability of the present calculations. The only exception to the described trend is YbS. The reason for this exception will be discussed later. Due to the larger ionic radius of sulfur compared to oxygen, the lattice constants of lanthanide monosulfides are significantly larger than those reported for the corresponding monoxides[7]. This structural expansion has direct consequences on their elastic response and high-pressure behavior.

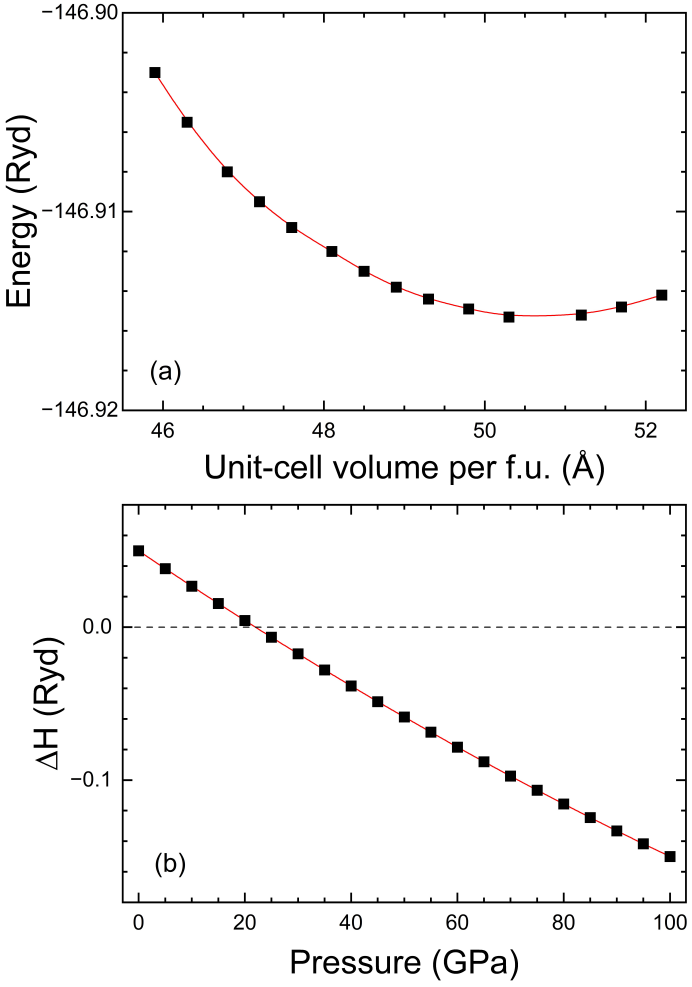

Figure 1 (a) Total energy vs volume per formula unit for B1-type LaS. The symbols are the results of calculations and the red line the Birch-Murnaghan fit. (b) Difference between the enthalpy of phases B1 and B2 ($\Delta H = H_{B2}$-H_{B1}) for LaS. The symbols are the results of calculations and the red line is a second-order polynomial fit. At P = 22 GPa H_{B2} becomes smaller than H_{B1}

Next, we compare our optimized equilibrium structures at 0 GPa with available experimental data. LaS has been extensively investigated experimentally[3,13,21–29], with an average reported lattice parameter for the B1 phase of $a = 5.860$ Å. This value is in excellent agreement with our calculated result of $a = 5.8839$ Å. For CeS, experimental data are more limited, with only three reported values of 5.778 Å[30], 5.77 Å[31], and 5.766 Å[32]. These values are approximately 1% smaller than our calculated lattice parameter, a discrepancy that remains within the typical accuracy of DFT calculations. A similar level of agreement is found for PrS, for which the average experimental lattice parameter reported in different studies[21,30,33–35] differs by about 1% from our theoretical value. For NdS, the experimental lattice parameter of 5.6975 Å[36] is likewise approximately 1% smaller than the present re-

View Article Online
DOI: 10.1039/D6DT00593D

sult. For the heavier lanthanide monosulfides -GdS, TbS, HoS, ErS, YbS, and LuS- the agreement between our calculated lattice parameters and available experimental measurements[30,37–44] is consistently very good. Overall, the close correspondence between theory and experiment across the lanthanide series confirms the reliability of the present computational approach and supports the validity of the observed systematic trends.

Figure 2(a) and Table 1 shows a clear trend across the lanthanide series: the unit-cell parameter of the B1 structure decreases with increasing atomic number. This behavior arises from the lanthanide contraction, caused by the progressive filling of the poorly shielding 4f orbitals. As a consequence, the ionic radius of Ln atoms decreases systematically, leading to shorter Ln–S bond lengths, increased bond strength, and higher charge density. These effects produce a more compact and cohesive crystal lattice, which is reflected in the observed reduction of the unit-cell parameters. The bulk modulus (Figure 2(b) and Table 1) also displays a smooth and nearly monotonic behavior. This parameter increases with increasing the atomic number of the lanthanide atoms, and it is also connected to the contraction of the 4f-electron shell, which strengthens the effective ionic bonding. Consequently, heavier lanthanide monosulfides are less compressible than lighter ones, in agreement with general trends observed in other rare-earth compounds[7]. When compared to lanthanide monoxides[7], the bulk moduli of lanthanide monosulfides is systematically smaller, indicating weaker bonding and enhanced structural softness associated with the lanthanide–sulfur interaction.

YbS is the only compound that deviates from the systematic trends described above. Similar anomalous behavior has previously been reported for YbO when compared to other lanthanide monoxides[7], as well as for elemental Yb relative to the rest of the lanthanide series[45,46]. This anomaly arises from the unique electronic configuration of ytterbium, which is the most compressible lanthanide because it adopts a stable divalent state at ambient pressure. In this state, Yb contributes only two valence electrons ($6s^2$) to bonding, in contrast to most lanthanides, which contribute three valence electrons ($6s^25d^1$). Thus Yb^{2+} has the same ionic radius[47] than Ce^{3+}. The reduced valence electron density of Yb leads to weaker bonding and a larger molar volume in YbS, resulting in an enhanced compressibility. Upon application of high pressure, Yb undergoes a gradual electronic transition to the trivalent state, strengthening the bonding and is accompanied by a significant volume reduction[48]. To verify that the anomalous behavior of YbS is not an artifact of freezing the 4f electrons, we performed additional calculations using a pseudopotential where the 4f states of Yb are treated explicitly as valence electrons. The obtained lattice parameter and bulk modulus agree with both approximations within 2%, remaining significantly different from the systematic trend observed for trivalent lanthanide sulfides, confirming that the anomaly originates from the divalent electronic configuration of Yb rather than from the computational approximation..

Figure 1(b) shows as an example the difference of enthalpy as a function of pressure between the B1 and B2 structures of LaS. At low pressures, the enthalpy of the B1 phase is less than that of

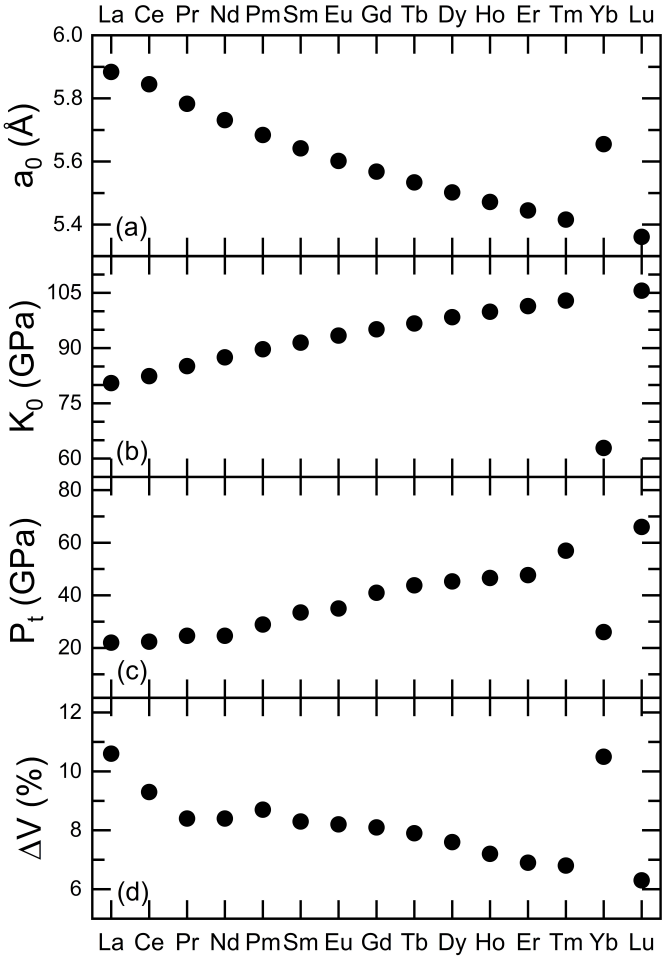

Figure 2 (a) Calculated equilibrium unit-cell parameter at 0 GPa (a_0). (b) Calculated bulk modulus K_0. (c) Calculated transition pressure (P_t). (d) Calculated relative change of the volume at the phase transition (Δ V). The LnS compounds are identified by the name of the lanthanide atom in the horizontal axes.

the B2 phase, suggesting that B1 is the most thermodynamically stable structure of the two up to a critical pressure. As pressure increases, the enthalpy difference between the two phases decreases, and eventually at 22 GPa it changes sign, with the B2 structure becoming energetically favored. This crossing unambiguously signals a pressure-induced structural phase transition from B1 to B2. The same behavior was found in all compounds studied here. Thus, all lanthanide monosulfides are found to be thermodynamically stable in the B1 structure at ambient conditions and to undergo a $B1 \rightarrow B2$ transition under compression. The transition pressures are summarized in Figure 2(c) and Table 1. In the table our results are compared with previous studies when available. The results agree with previous studies for LaS[8], CeS[12], and PrS[9] (see Table 1). The good agreement between our results and those previously obtained using different methods strengthens the robustness and reliability of our conclusions. The lower transition pressures reported in previous studies for EuS and YbS (see Table 1), compared to the present results, likely reflect methodological limitations, including the tendency of self-interaction-corrected schemes to overstabilize high-density

View Article Online
DOI: 10.1039/D6DT00593D

Table 1 Calculated unit-cell parameter, bulk modulus and pressure derivative of the bulk modulus at 0 GPa for the B1 and B2 structures. We also report the calculated pressure for the phase transition from B1 to B2 and the relative change of volume at the transition pressure. Results are compared with the literature.

	Type B1			Type B2			This work		Literature			
Studied LnS	a_0 [Å]	K_0 [GPa]	K_0'	a_0 [Å]	K_0 [GPa]	K_0'	P_t [GPa]	$\Delta V/V_0$ [%]	P_t [GPa]	$\Delta V/V_0$ [%]	K_0 [GPa]	Ref.
LaS	5.884	80.5	4.47	3.580	77.5	4.18	22.0	10.6	24.9	8.4	87-107	[8]
CeS	5.845	82.4	4.47	3.569	80.9	4.34	22.4	9.3	24.3	7	79	[12]
PrS	5.783	85.1	4.48	3.534	83.3	4.36	24.6	8.4	22	10	89-107	[9]
NdS	5.731	87.5	4.48	3.505	85.3	4.32	24.6	8.4				
PmS	5.684	89.7	4.39	3.480	87.3	4.24	28.9	8.7				
SmS	5.642	91.5	4.40	3.458	89.0	4.36	33.5	8.3	0.1-1.24	11.1-13.8	53.4	[10]
EuS	5.602	93.4	4.40	3.437	90.3	4.30	35.0	8.2	11.6-21.5	5.7-12.5	53.6-63	[11,12]
GdS	5.568	95.1	4.41	3.420	91.5	4.30	41.0	8.1				
TbS	5.534	96.7	4.40	3.403	92.5	4.26	43.8	7.9				
DyS	5.502	98.4	4.39	3.387	93.6	4.28	45.3	7.6				
HoS	5.472	99.9	4.36	3.373	94.2	4.25	46.6	7.2				
ErS	5.445	101.4	4.39	3.361	95.8	4.27	42.7	6.9				
TmS	5.416	102.9	4.36	3.347	96.4	4.26	57.0	6.8				
YbS	5.655	62.9	4.10	3.427	65.1	4.07	26.0	10.5	9.4	15.1	51.3-74	[12]
LuS	5.361	105.6	4.38	3.321	99.3	4.25	66.0	6.3				

phases[49] and the treatment of three-body interactions in YbS[50]. In the case of SmS, the apparent discrepancies between our results and previous work[10] can be attributed to the fact that the earlier study focused on an isostructural phase transition rather than the B1–B2 transition. According to our results, the transition pressure and the change of volume at the phase transition increase when moving from La to Lu as shown in Figure 2(c) and 2(d). The same trend was previously found in lanthanide monoxides[7]. We also noticed that according to our results, lanthanide sulfides exhibit systematically smaller transition pressures than the corresponding lanthanide monoxides, indicating that the structural phase transitions in sulfides occur more readily under compression.

Regarding the bulk modulus, we find good agreement with previous studies for LaS[8], CeS[12], and PrS[9]. In contrast, earlier studies on SmS[10], EuS[11], and YbS[12] report smaller bulk moduli than those obtained in the present work (see Table 1). These discrepancies likely originate from the same methodological differences discussed in the previous paragraph for the transition pressures. The bulk modulus follows a systematic behavior as shown in Figure 2(b) and Table 1. The increase of the bulk modulus when moving from La to Lu is consistent with the decrease of the unit-cell volume. the more dense a material the lesser compressible. In addition, we found that the calculated bulk moduli of lanthanide sulfides are lower than those of lanthanide monooxides, implying that sulfides are more compressible and mechanically softer. This combined behavior originates from the weaker bonding and larger anion size in sulfides compared to oxides, which reduces resistance to volume change. As a result, lower pressures are required to stabilize the B2 phase. The difference in the behavior between lanthanide monosulfides and lanthanide monoxides is similar to the conclusions from the comparison between the behavior of alkaline-earth sulfides and oxides. CaS has a lower transition pressure (around 36.5 GPa) than CaO (between 53–70 GPa)[51,52]. The same qualitative difference can be found in strontium compounds. The transition pressure for Sr is significantly higher (36-38 GPa)[53] than for strontium SrS, which transitions around 18 GPa[54]. In Barium compounds, BaS has a single transition from the B1 to the B2 phase at approximately 6.5 GPa[55,56], while BaO undergoes a more complex series of transitions starting from B1 and reaching a distorted CsCl-type roughly 15.0 GPa[56]. Finally, the same differences occur between MgO and MgS. MgS goes from the zinc-blende (B3) structure to the B1 structure at approximately 2.9 GPa, and from the B1 structure to the B2 structure transition in the range of 158-255.5 GPa[57]. The transition pressure for MgO from B1 to B2 occurs approximately at 400–600 GPa[58].

It is also instructive to compare these results with yttrium sulfide (YS), which, although not a lanthanide compound, is often considered a useful reference due to its similar ionic radius and the absence of 4f electrons. Previous studies have shown that YS undergoes a B1–B2 structural transition under pressure, following a trend comparable to that of early lanthanide monosulfides[59]. The transition pressure for YS was calculated to be 53 GPa, which lies within the range observed for lanthanide sulfides (from 20 GPa for LaS to 60 GPa for LuS). Although yttrium is not a lanthanide, its transition pressure closely matches that of LuS. This is unsurprising because Lu has a complete 4f electron shell ($[Xe]4f^{14}5d^{1}6s^{2}$) and Y has a $[Kr]4d^{1}5s^{2}$ configuration. The 4f electrons in Lu have minimal influence on high-pressure behavior because the 4f shell is fully filled, making them largely inert and not contributing significantly to bonding or the structural transition. So the transition pressure of LuS is largely determined by the response of the d and s electrons, as in YS. Additionally, the similar ionic radii of Y^{3+} (0.90 Å) and Lu^{3+} (0.86 Å) support the comparable transition pressures. Consequently, the similarities in electronic configuration and ionic size lead to analogous structural and bonding characteristics under pressure for both com-

View Article Online
DOI: 10.1039/D6DT00593D

pounds. This is further reflected in the the fact that the unit-cell parameters and bulk moduli exhibit close agreement between the two compounds. Lattice constants are 5.489 Å for YS and 5.361 Å for LuS (2% difference), and bulk moduli are 93–101.4 GPa for YS [59] and 105.6 GPa for LuS.

To conclude this section, we would like to comment on the fact that our calculations were carried out at 0 K. While our enthalpy calculations suggest a first-order phase transition from B1 to B2 under pressure, we acknowledge that phononic entropy may also contribute significantly to the thermodynamic behavior. The pressure-induced changes in the phonon density of states and their corresponding entropy could influence the transition, potentially smoothing or altering its apparent order. However, detailed finite-temperature studies, which are beyond the scope of this work, could further explore these effects. These phononic contributions are unlikely to affect the systematic behavior discussed here. We would also like to comments that the approximate treatment of exchange–correlation effects, and the neglect of zero-point and finite-temperature vibrational contributions, could affect the transition. However, these effects mainly influence the absolute transition pressure, while the consistent computational treatment ensures that the predicted trends across the lanthanide series remain robust and physically meaningful.

3.2 Elastic constants

Elastic constants are critical for determining the mechanical stability, stiffness, and bonding properties of crystalline materials. The strain-stress method, described in the thermo_pw code [20], is used to calculate the three independent elastic constants (C_{11}, C_{12}, C_{44}) of the B1 and B2 phases of lanthanide monosulfides. This method involves applying small strains to the crystal lattice, resulting in a total relaxation of the lattice containing the atoms and determining the corresponding stress. The calculated elastic constants are given in Table 2 for the B1 phase and in Table 3 for the B2 phase. The calculated elastic constants for LaS show good agreement with the values reported in Refs. 13 and 28, supporting the reliability of the present approach. As can be seen from Table 2 and Table 3, the values of C_{11} for all investigated compounds are significantly larger than those of C_{44}, suggesting a weaker resistance to pure shear deformation compared to unidirectional compression. For mechanical stability, the generalized Born–Huang criteria [60,61] stipulate that a cubic crystal must satisfy the following conditions: $C_{44} - P > 0$, $C_{11} - C_{12} + P > 0$, and $(C_{11} + 2C_{12}) + P > 0$. In the pressure range of stability of the B1 and B2 phases, the calculated elastic constants for all investigated compounds are positive and meet the necessary conditions for mechanical stability. The Cauchy pressure ($C_p = C_{12} - C_{44}$) is commonly used to determine the ductility or brittleness of metallic compounds [62]. Positive (negative) values of C_p suggest ductile (brittle) behavior. All studied compounds have positive C_p values, suggesting ductile behavior, except for YbS in the B1 phase, which has a negative value and is therefore brittle.

The Voigt-Reuss-Hill scheme [63–65] is applied to calculate the isotropic bulk and shear moduli (B_{VRH}, G_{VRH}), in as well as Young's modulus (E) and Poisson's ratio (σ). The Voigt [63] and Reuss [64] schemes assume uniform strain and uniform stress, respectively, giving the upper and lower limits of the elastic moduli of polycrystals. The Hill average [65] is the most reliable estimate of the mechanical properties based on single-crystal elastic constants. The general Voigt-Reuss-Hill (VRH) equations for cubic crystals are given as follows [63–65]:

$$B_V = B_R = \frac{C_{11} + 2C_{12}}{3}, \tag{1}$$

$$G_V = \frac{C_{11} - C_{12} + 3C_{44}}{5}, \tag{2}$$

$$G_R = \frac{5C_{44}(C_{11} - C_{12})}{4C_{44} + 3(C_{11} - C_{12})}, \tag{3}$$

$$B_H = \frac{B_V + B_R}{2}, \tag{4}$$

$$G_H = \frac{G_V + G_R}{2}, \tag{5}$$

$$E = \frac{9B_H G_H}{3B_H + G_H}, \tag{6}$$

$$\sigma = \frac{3B_H - E}{6B_H}. \tag{7}$$

The calculated values of the bulk modulus (B_H), shear modulus (G_H), Young's modulus (E), the bulk-to-shear modulus ratio (B_H/G_H), and Poisson's ratio (σ) are shown in Table 2 and Table 3. The bulk modulus (B_H) describes the resistance of a material to volume change under applied pressure, whereas the shear modulus (G_H) implies the resistance to shape deformation induced by shear stress.

Table 2 and Table 3 show that LuS has larger bulk and shear moduli in both phases (B1 and B2) compared to other compounds studied, indicating that this compound has a better capability of resistance to volume change as well as shape change. In contrast, PmS in the B1 phase and for LaS in the B2 phase have the weakest resistance to volume and shape deformations, due to their smallest B_H and G_H values. Young's modulus (E) is closely related to solid stiffness; a higher E value suggests a stiffer material. Among all the studied compounds, LuS in the B1 phase and PmS in the B2 phase have the highest E values, indicating that they are the stiffest compounds in their respective phases. In addition to the Cauchy pressure, Pugh [66] suggested the ratio of the bulk modulus to the shear modulus (B_H/G_H) as a criterion for identifying between ductile and brittle behavior. If this ratio exceeds a critical value of 1.75, the material is expected to be ductile; otherwise, it is considered as brittle. In agreement with the Cauchy pressure criteria, all studied compounds exhibit $B_H/G_H > 1.75$, except YbS, hence confirming their ductile properties.

In addition to the elastic moduli, the longitudinal (v_L), transverse (v_T), and average elastic wave velocities (v_M) supply additional understanding of the elastic and mechanical properties of solids. These velocities have an inherent connection to the bulk and shear moduli, as well as the density of the material, and they are crucial for characterizing lattice dynamics and the strength of

View Article Online
DOI: 10.1039/D6DT00593D

Table 2 The second-order elastic constants (C_{11}, C_{12}, C_{44}), the isotropic bulk modulus (B_H), shear modulus (G_H), Young's modulus (E), B_H/G_H ratio, and Poisson's ratio (σ), the transverse (v_T), longitudinal (v_L) and average elastic wave velocities (v_M) for the B1 phase of LnS compounds.

Compound	C_{11} (GPa)	C_{12} (GPa)	C_{44} (GPa)	B_H (GPa)	G_H (GPa)	E (GPa)	B_H/G_H	σ	v_L (m/s)	v_T (m/s)	v_M (m/s)
LaS	191.60	24.96	22.62	80.50	39.42	101.21	2.04	0.284	4885.4	2659.0	3800.0
CeS	200.43	23.37	17.60	82.39	35.93	93.31	2.29	0.298	4770.5	2505.3	3793.3
PrS	208.25	23.65	18.41	85.18	37.52	97.30	2.27	0.297	4771.3	2513.4	3787.1
NdS	214.79	23.95	19.16	87.57	38.92	100.82	2.25	0.295	4734.1	2500.9	3751.3
PmS	196.70	22.14	19.83	80.33	37.76	97.28	2.13	0.288	4572.7	2458.1	3585.2
SmS	225.73	24.58	20.45	91.63	41.25	106.70	2.22	0.293	4662.5	2473.1	3685.6
EuS	230.59	24.97	21.04	93.51	42.29	109.35	2.21	0.293	4644.0	2466.9	3667.9
GdS	235.01	25.33	21.42	95.22	43.11	111.42	2.21	0.292	4577.9	2432.3	3615.1
TbS	239.20	25.75	21.75	96.90	43.83	113.30	2.21	0.292	4555.6	2419.9	3598.0
DyS	243.21	26.23	22.02	98.56	44.46	114.97	2.22	0.293	4510.0	2393.7	3563.8
HoS	246.94	26.71	22.13	100.12	44.92	116.23	2.23	0.294	4476.0	2371.6	3540.5
ErS	250.33	27.24	21.98	101.60	45.09	116.79	2.25	0.295	4440.7	2344.9	3519.7
TmS	253.82	27.78	21.95	103.13	45.39	117.65	2.27	0.296	4412.6	2323.8	3503.0
YbS	147.09	20.15	34.55	62.46	44.18	107.23	1.41	0.213	4012.6	2421.0	2878.6
LuS	260.07	28.93	21.53	105.98	45.53	118.31	2.33	0.299	4321.4	2258.5	3445.7

Table 3 The second-order elastic constants (C_{11}, C_{12}, C_{44}), the isotropic bulk modulus (B_H), shear modulus (G_H), Young's modulus (E), B_H/G_H ratio, and Poisson's ratio (σ), the transverse (v_T), longitudinal (v_L) and average elastic wave velocities (v_M) for the B2 phase of LnS compounds.

Compound	C_{11} (GPa)	C_{12} (GPa)	C_{44} (GPa)	B_H (GPa)	G_H (GPa)	E (GPa)	B_H/G_H	σ	v_L (m/s)	v_T (m/s)	v_M (m/s)
LaS	146.97	43.77	32.64	78.17	39.24	100.85	1.99	0.284	4593.0	2518.8	3554.9
CeS	151.19	45.12	36.42	80.47	42.35	108.10	1.90	0.276	4666.0	2594.9	3576.8
PrS	156.98	46.17	36.59	83.10	43.23	110.52	1.92	0.278	4649.8	2577.0	3573.0
NdS	162.08	46.81	36.01	85.23	43.52	111.56	1.96	0.281	4590.1	2529.9	3540.5
PmS	166.73	47.18	35.07	87.03	43.48	111.81	2.00	0.285	4559.7	2496.9	3532.5
SmS	171.26	47.52	33.86	88.77	43.21	111.51	2.05	0.290	4470.7	2428.9	3481.5
EuS	165.28	42.67	28.58	83.54	39.01	101.20	2.14	0.297	4283.3	2297.7	3362.6
GdS	179.56	47.84	30.78	91.75	41.96	109.18	2.19	0.301	4335.0	2310.7	3416.6
TbS	183.22	47.87	28.93	92.99	40.97	107.10	2.27	0.306	4283.2	2256.6	3399.4
DyS	186.56	47.74	26.87	94.01	39.74	104.38	2.37	0.313	4205.7	2186.8	3363.3
HoS	189.50	47.56	24.67	94.88	38.29	101.08	2.48	0.319	4138.4	2119.8	3336.9
ErS	191.88	47.45	22.39	95.59	36.62	97.20	2.61	0.326	4071.3	2050.3	3312.2
TmS	194.96	47.22	20.05	96.46	34.94	93.21	2.76	0.333	4009.8	1981.7	3292.7
YbS	139.56	37.84	30.78	63.75	41.96	109.18	1.52	0.201	4954.0	2712.0	3838.7
LuS	200.69	46.50	15.13	99.94	41.98	83.80	2.38	0.346	3854.0	1820.8	3230.0

bonding. As shown in Table 2 and Table 3, LuS shows relatively lower elastic wave velocities in both the B1 and B2 phases compared to the other compounds. This behavior can be explained by its larger atomic mass and higher density, which decrease the velocities of elastic waves despite its comparatively large elastic moduli. Elastic constant analysis reveals that the B1 (NaCl-type) phase generally has higher C_{44} and shear modulus (G_H) values compared to the B2 (CsCl-type) phase, thus supporting its increased shear resistance, especially among the heavier lanthanides. However, YbS in the B1 phase is a notable anomaly. Its anomalously low shear stiffness, negative Cauchy pressure, and brittle behavior result from the weak, isotropic bonding of the divalent Yb^{2+} ion, which undermines the directional strength characteristic of the NaCl-type structure.

3.3 Phonons

Phonon dispersion relations and phonon density of states are crucial quantities for characterizing lattice dynamics and determining the dynamical stability of crystalline materials. Here, we examine the phonon spectra of lanthanide monosulfides in both the B1 phase at 0 GPa and in the B2 phase at the corresponding transition pressure to better understand their vibrational properties and the stability of these phases under pressure. Before presenting the results we would like to comment that a known limitation of standard DFT approaches is their reduced accuracy in describing lattice dynamics in systems containing localized 3d or 4f electrons. Previous studies on rare-earth and transition-metal compounds have shown that conventional approximations often lead to a systematic underestimation of phonon frequencies, particularly in the optical branches, due to an incomplete treatment of electronic correlations and electron–phonon coupling involv-

View Article Online
DOI: 10.1039/D6DT00593D

ing localized states[67,68]. Nevertheless, despite these quantitative discrepancies at the level of individual phonon modes, the overall features of the phonon spectra - such as dispersion trends, acoustic–optical separation, and dynamical stability - are typically well reproduced[67,68]. In this context, earlier investigations of rare-earth chalcogenides have demonstrated that DFT provides a reliable description of global vibrational properties and their evolution under pressure, even when subtle spectral details are not perfectly captured. Therefore, while the present calculations may inherit similar limitations associated with the treatment of 4f electrons, they are expected to yield robust and physically meaningful trends across the lanthanide series, particularly regarding structural stability, relative phase behavior, and general characteristics of the phonon spectra.

The primitive cell of the B1 and B2 phases of lanthanide monosulfides consists of two atoms, resulting in six vibrational modes, three of which are acoustic and three optical. According to group theory, the zone-center optical phonon modes of the B1 and B2 phases correspond to the T_{1u} irreducible representation of the O_h ($m\bar{3}m$) point group, resulting in a triply degenerate infrared-active mode. Table 4 shows the calculated zone-center T_{1u} optical phonon frequencies for the B1 and B2 phases of lanthanide monosulfides. The B1 phases have higher T_{1u} frequencies compared to the B2 phases, suggesting the higher stiffness of the NaCl-type lattice in comparison to the CsCl-type lattice. The table shows that, for all compounds, the vibrations are largely determined by the lighter sulfur atoms, whereas the heavier lanthanide atoms contribute weakly to each mode.

The phonon dispersion curves for the B1 and B2 phases of lanthanide monosulfides are shown in Figs. 3 and 4, respectively. The absence of imaginary phonon modes proves the dynamical stability of all studied B1 and B2 phases of lanthanide monosulfides. The large mass difference between lanthanide atoms and sulfur leads to a significant gap between the acoustic and optical phonon branches for B1 phase, as shown in Fig. 3. The phonon spectra of the B1 phases show a similar behavior for the lanthanide monosulfides, as seen in Fig. 3. An exception is YbS, where the acoustic phonon branches reach roughly 4 THz, while the maximum acoustic frequencies for other lanthanide monosulfides are around 3 THz. This indicates that YbS has comparatively higher acoustic phonon frequencies. The optical phonon branches of YbS show a wider frequency range than those of other compounds, with its lowest optical phonon frequency having the lowest among all materials studied, reaching at around 5.6 THz. Thus, YbS has the smallest acoustic–optical phonon gap among the lanthanide monosulfides. A large mass difference between lanthanide atoms and sulfur generally suggests an increase in the acoustic–optical phonon gap; however, the decreased gap in YbS implies that mass effects alone are not sufficient explanations for its vibrational properties. This anomaly can be explained to the decreased interatomic bonding in YbS, matching with its elastic properties. The extremely small shear modulus, decreased C_{44} value, and negative Cauchy pressure found for YbS in the B1 phase indicate weak and less directional bonding related to the divalent Yb^{2+} electronic configuration. The weaker force constants decrease the optical phonon frequencies and dominate over mass effects, leading to a reduced phonon gap for YbS.

Table 4 The calculated zone-center optical phonon frequencies (ν in cm^{-1}) and eigen characteristics for lanthanide monosulfides. IR denotes infrared-active vibrations. We show in bold characters the atom that contributes most to each vibration. The symmetry assignment of each mode is included.

Compound	Phase	Mode	ν (cm^{-1})	Eigen characters
LaS	B1	T_{1u} (IR)	251.95	**S**+La
CeS	B1	T_{1u} (IR)	251.99	**S**+Ce
PrS	B1	T_{1u} (IR)	256.08	**S**+Pr
NdS	B1	T_{1u} (IR)	259.00	**S**+Nd
PmS	B1	T_{1u} (IR)	249.57	**S**+Pm
SmS	B1	T_{1u} (IR)	263.76	**S**+Sm
EuS	B1	T_{1u} (IR)	266.13	**S**+Eu
GdS	B1	T_{1u} (IR)	267.53	**S**+Gd
TbS	B1	T_{1u} (IR)	269.34	**S**+Tb
DyS	B1	T_{1u} (IR)	270.82	**S**+Dy
HoS	B1	T_{1u} (IR)	272.23	**S**+Ho
ErS	B1	T_{1u} (IR)	273.42	**S**+Er
TmS	B1	T_{1u} (IR)	274.71	**S**+Tm
YbS	B1	T_{1u} (IR)	183.18	**S**+Yb
LuS	B1	T_{1u} (IR)	276.65	**S**+Lu
LaS	B2	T_{1u} (IR)	173.87	**S**+Lu
CeS	B2	T_{1u} (IR)	171.17	**S**+Ce
PrS	B2	T_{1u} (IR)	172.77	**S**+Pr
NdS	B2	T_{1u} (IR)	173.16	**S**+Nd
PmS	B2	T_{1u} (IR)	173.49	**S**+Pm
SmS	B2	T_{1u} (IR)	173.13	**S**+Sm
EuS	B2	T_{1u} (IR)	163.94	**S**+Eu
GdS	B2	T_{1u} (IR)	172.34	**S**+Gd
TbS	B2	T_{1u} (IR)	171.75	**S**+Tb
DyS	B2	T_{1u} (IR)	170.77	**S**+Dy
HoS	B2	T_{1u} (IR)	169.62	**S**+Ho
ErS	B2	T_{1u} (IR)	168.27	**S**+Er
TmS	B2	T_{1u} (IR)	167.39	**S**+Tm
YbS	B2	T_{1u} (IR)	223.82	**S**+Yb
LuS	B2	T_{1u} (IR)	164.99	**S**+Lu

A comparison of the phonon dispersion relations between both phases reveals significant and systematic differences among the lanthanide monosulfides. In the B1 phase, a distinctive frequency gap between the acoustic and optical phonon branches appears for all lanthanide monosulfides. In the transition to the B2 phase, the acoustic–optical phonon gap vanishes for all compounds except LaS. In LaS, the gap does not completely disappear but decreases significantly from approximately 6 THz in the B1 phase to about 0.2 THz in the B2 phase. Thus, the acoustic and optical branches are interconnected within the B2 phase. The reduction of the acoustic–optical phonon gap in the B2 phase reflects stronger vibrational coupling under compression. This behavior is expected under compression, as increased pressure enhances interatomic interactions and induces stronger coupling between vibrational modes, leading to the closure of the phonon gap. Furthermore, the highest phonon frequencies usually decrease in the B2 phase compared to the B1 phase for all compounds, except for the YbS. The overall decrease in the highest phonon frequencies signifies a softening of lattice vibrations in the B2 structure,

View Article Online
DOI: 10.1039/D6DT00593D

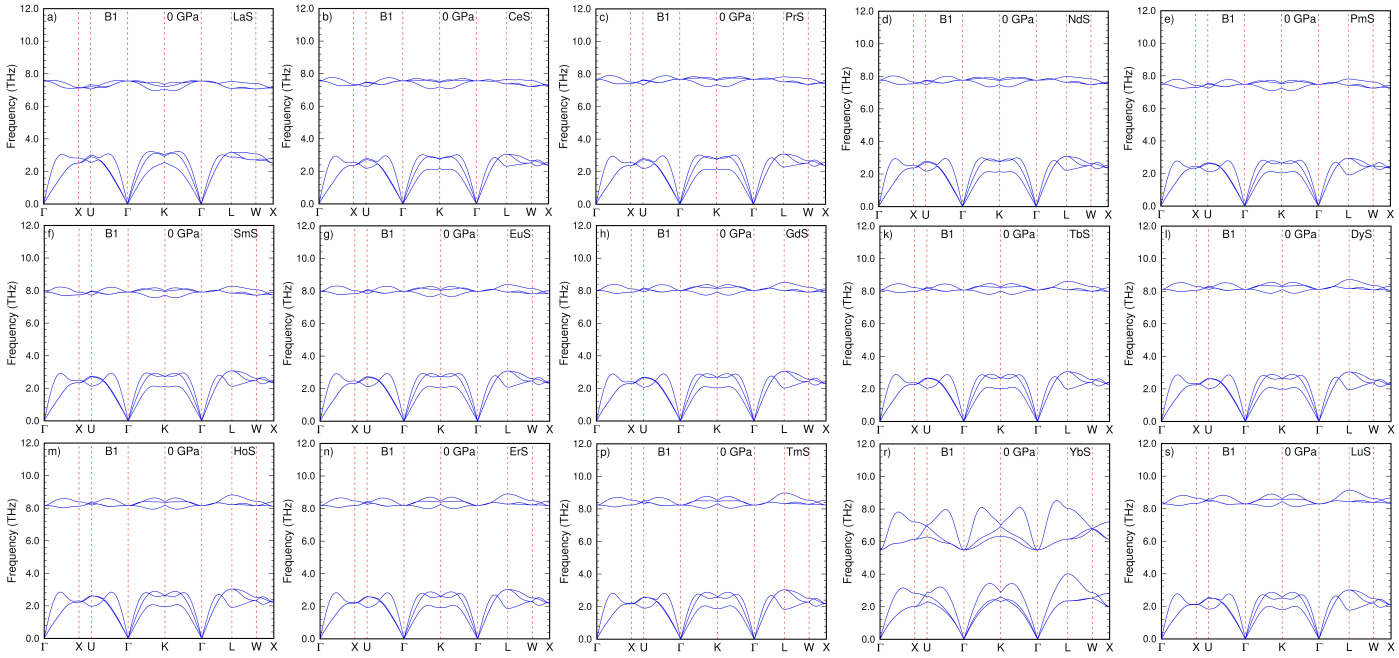

Figure 3 The calculated phonon dispersion curves for the B1 phase of lanthanide monosulfides. (a) LaS, (b) CeS, (c) PrS, (d) NdS, (e) PmS, (f) SmS, (g) EuS, (h) GdS, (k) TbS, (l) DyS, (m) HoS, (n) ErS, (p) TmS, (r) YbS, (s) LuS at 0 GPa. Each panel shows the dispersion along the high-symmetry directions of the Brillouin zone.

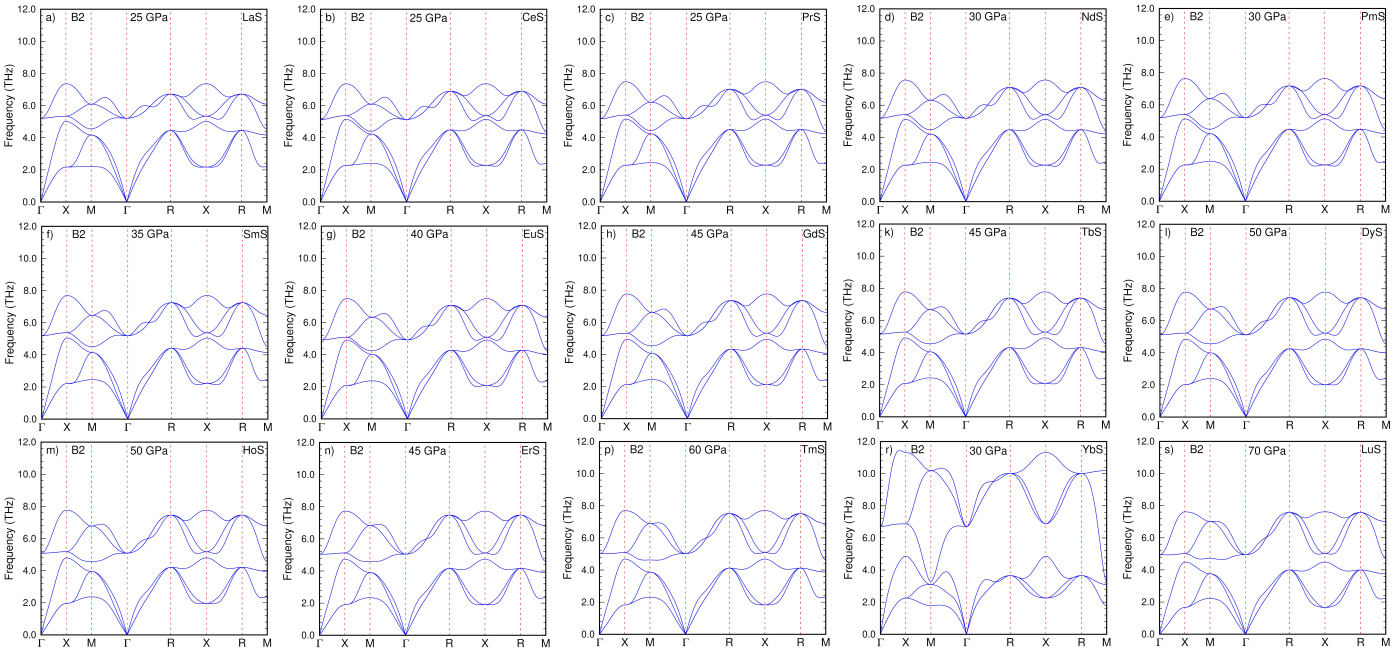

Figure 4 The calculated phonon dispersion curves for the B2 phase of lanthanide monosulfides. (a) LaS, (b) CeS, (c) PrS, (d) NdS, (e) PmS, (f) SmS, (g) EuS, (h) GdS, (k) TbS, (l) DyS, (m) HoS, (n) ErS, (p) TmS, (r) YbS, (s) LuS at the pressures given in the plots, which are slightly larger than the corresponding transition pressures. Each panel shows the dispersion along the high-symmetry directions of the Brillouin zone.

View Article Online
DOI: 10.1039/D6DT00593D

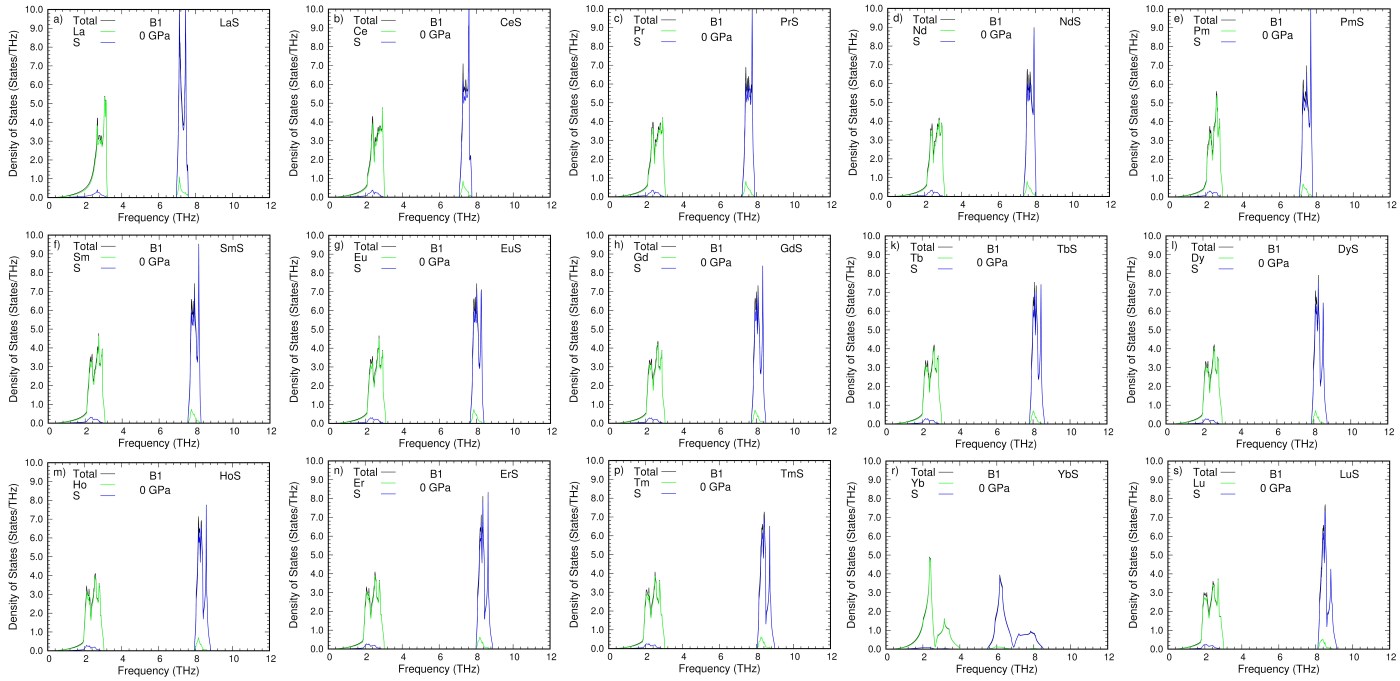

Figure 5 The calculated total and partial phonon density of states for the B1 phase of lanthanide monosulfides. (a) LaS, (b) CeS, (c) PrS, (d) NdS, (e) PmS, (f) SmS, (g) EuS, (h) GdS, (k) TbS, (l) DyS, (m) HoS, (n) ErS, (p) TmS, (r) YbS, (s) LuS at 0 GPa.

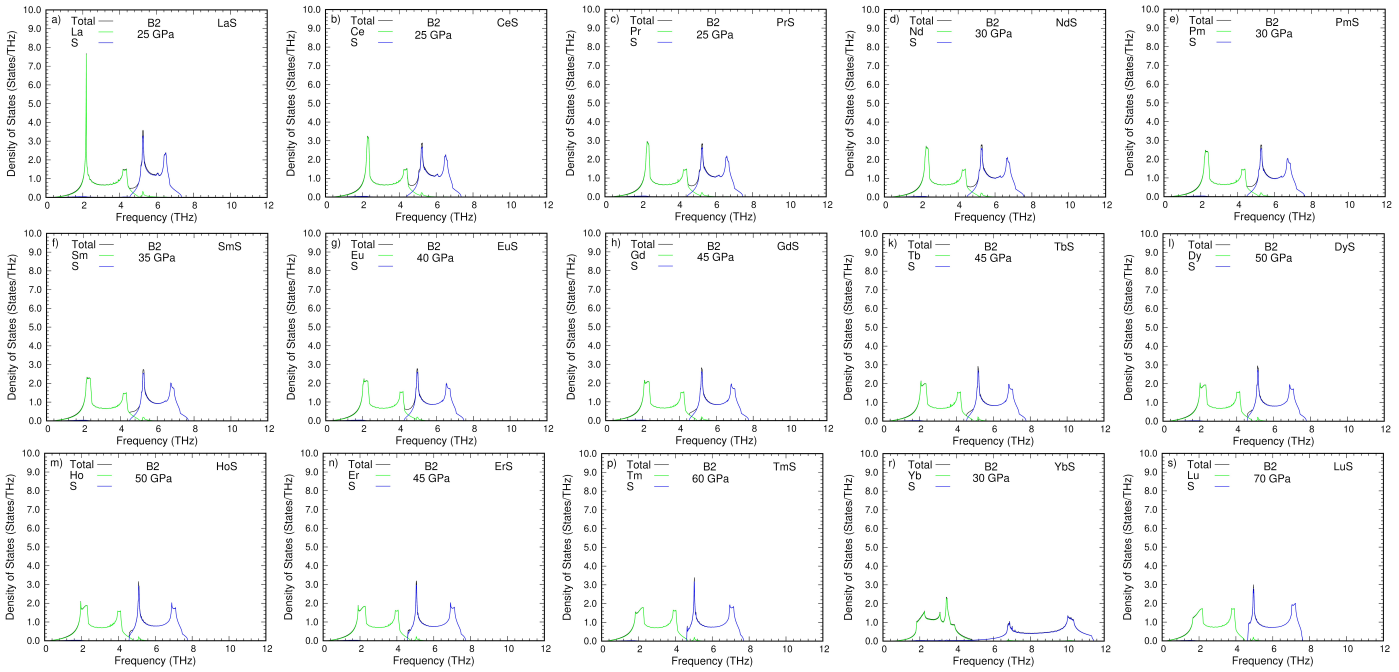

Figure 6 The calculated total and partial phonon density of states for the B2 phase of lanthanide monosulfides. (a) LaS, (b) CeS, (c) PrS, (d) NdS, (e) PmS, (f) SmS, (g) EuS, (h) GdS, (k) TbS, (l) DyS, (m) HoS, (n) ErS, (p) TmS, (r) YbS, (s) LuS at the pressures given in the plots, which are slightly larger than the corresponding transition pressures.

View Article Online
DOI: 10.1039/D6DT00593D

corresponding with its higher compressibility and decreased effective bonding compared to the B1 phase, as also suggested by the elastic constant analysis. The B2 phase thus shows softer phonon modes despite the applied pressure, indicating decreased directional bonding in the CsCl-type structure. YbS provides an unusual anomaly within the lanthanide monosulfide series. In contrast to the other compounds, the highest phonon frequency of YbS has a notable increase throughout the B1–B2 transition, shifting from approximately 8.6 THz to 11.6 THz. Furthermore, the acoustic and optical phonon branches in the B2 phase show a wider frequency range for all studied compounds compared to the B1 phase. This wider dispersion indicates increased phonon anharmonicity and a more complex vibrational environment in the high-pressure B2 structure, emphasizing the crucial differences in lattice dynamics between the two phases.

The total and partial phonon density of states (PhDOS) of the B1 and B2 phases are shown in Figs. 5 and 6. This allows us to identify the contributions of all the phonon modes to the total phonon spectrum. The acoustic phonon modes mainly originate from the heavier lanthanide atoms, whereas the high-frequency optical modes are dominated by the vibrations of the lighter sulfur atoms. In the B2 phases, the peak values of the phonon density of states are significantly decreased, suggesting a more uniform vibrational spectrum, which can be due to the increased structural symmetry of the B2 phase compared to B1.

4 Conclusions

In this work, the structural, elastic, and vibrational properties of lanthanide monosulfides (LnS, Ln = La–Lu) under pressure have been systematically investigated using first-principles calculations within the framework of density functional theory. The equilibrium structural parameters obtained for the B1 (NaCl-type) phase are in good agreement with available experimental and theoretical data, confirming the reliability of the computational approach used in this study.

A clear systematic evolution of structural properties across the lanthanide series is observed as a consequence of the lanthanide contraction. The calculated lattice parameters decrease progressively from LaS to LuS, while the bulk moduli show a corresponding increase, indicating a gradual stiffening of the lattice with increasing atomic number. These trends reflect the reduction of ionic radii associated with the progressive filling of the 4f orbitals.

The pressure-induced structural transition from the B1 (NaCl-type) phase to the B2 (CsCl-type) phase has been examined for the entire LnS series. The calculated transition pressures exhibit a systematic increase along the series, demonstrating that the stability of the B1 structure relative to the B2 phase is strongly influenced by the lanthanide contraction. Among the compounds studied, YbS displays a noticeable deviation from the general trend, which can be attributed to the particular stability of the divalent ytterbium electronic configuration.

Elastic-constant calculations confirm that both the B1 and B2 phases satisfy the mechanical stability criteria within their respective pressure ranges. The evolution of the elastic constants and related mechanical properties further reflects the strengthening of interatomic interactions across the lanthanide series. In addition, phonon dispersion calculations demonstrate the dynamical stability of the structures in their stable pressure domains and reveal systematic variations in lattice vibrational behavior under compression.

Because experimental high-pressure data are currently available for only a limited number of lanthanide monosulfides, the results presented here provide predictive insights into the structural stability and phase-transition behavior of the entire LnS family. The systematic trends identified in this work highlight the dominant role of lanthanide contraction and electronic configuration in determining the structural and mechanical properties of rare-earth sulfides. These findings offer a useful theoretical reference for future experimental investigations of lanthanide chalcogenides under high-pressure conditions and contribute to a broader understanding of structure–property relationships in rare-earth compounds.

Author contributions

S. Ferrari, E. Karaca, and D. Errandonea: Investigation (equal); Methodology (equal); Writing - review & editing (equal).

Conflicts of interest

The authors have no conflicts to disclose.

Data availability

The data that support the findings of this article are available from the authors upon reasonable request.

Acknowledgments

D.E. thanks funding from Spanish Ministerio de Ciencia, Innovación y Universidades, through AEI (MCIN/AEI/10.13039/501100011033), and EU under grant PID2022-138076NB-C41.

References

1 M. Cahay, P. Boolchand, S. B. Fairchild, L. Grazulis, P. T. Murray, T. C. Back, V. Semet, V. T. Binh, X. Wu, D. Poitras, D. J. Lockwood, F. Yu and V. Kuppa, *J. Vacuum Sci. Techn. B*, 2011, **29**, 06F602.
2 U. Benedict, *J. Alloys Compd.*, 1995, **223**, 216–225.
3 W. Beckenbaugh, J. Evers, G. Güntherodt, E. Kaldis and P. Wachter, *J. Phys. Chem. Solids*, 1975, **36**, 239–248.
4 R. Didchenko and L. M. Litz, *J. Electr. Soc.*, 1962, **109**, 247.
5 S. Hirai, E. Sumita, K. Shimakage, Y. Uemura, T. Nishimura and M. Mitomo, *J. Amer. Ceram. Soc.*, 2004, **87**, 23–28.
6 R. Amano and Y. Shiokawa, *J. Rad. Nuclear Chem.*, 1991, **155**, 201–210.
7 S. Ferrari and D. Errandonea, *Crystals*, 2024, **14**, 83.
8 G. Vaitheeswaran, V. Kanchana and M. Rajagopalan, *Journal of Physics and Chemistry of Solids*, 2003, **64**, 15–26.
9 G. Vaitheeswaran, L. Petit, A. Svane, V. Kanchana and M. Rajagopalan, *Journal of Physics: Condensed Matter*, 2004, **16**, 4429.
10 A. Svane, V. Kanchana, G. Vaitheeswaran, G. Santi, W. M.

View Article Online
DOI: 10.1039/D6DT00593D

Temmerman, Z. Szotek, P. Strange and L. Petit, *Phys. Rev. B*, 2005, **71**, 045119.
11 A. Svane, G. Santi, Z. Szotek, W. M. Temmerman, P. Strange, M. Horne, G. Vaitheeswaran, V. Kanchana, L. Petit and H. Winter, *physica status solidi (b)*, 2004, **241**, 3185–3192.
12 R. Dubey and S. Singh, *J. Optoelect. Adv. Mat.*, 2014, **16**, 1328–1338.
13 G. Vaitheeswaran, V. Kanchana, S. Heathman, M. Idiri, T. Le Bihan, A. Svane, A. Delin and B. Johansson, *Phys. Rev. B*, 2007, **75**, 184108.
14 A. Liang, R. Turnbull and D. Errandonea, *Progress in Materials Science*, 2023, **136**, 101092.
15 H.-K. Mao, B. Chen, J. Chen, K. Li, J.-F. Lin, W. Yang and H. Zheng, *Matter and Radiation at Extremes*, 2016, **1**, 59–75.
16 Y. Luo, X. Wan, Y. Ito, S. Takami, M. Kubo and A. Miyamoto, *Chem. Phys.*, 2002, **282**, 197–206.
17 E. Karaca and D. Errandonea, *Dalton Trans.*, 2025, **54**, 14199–14213.
18 P. Giannozzi, S. Baroni, N. Bonini, M. Calandra, R. Car, C. Cavazzoni, D. Ceresoli, G. L. Chiarotti, M. Cococcioni, I. Dabo, A. Dal Corso, S. de Gironcoli, S. Fabris, G. Fratesi, R. Gebauer, U. Gerstmann, C. Gougoussis, A. Kokalj, M. Lazzeri, L. Martin-Samos, N. Marzari, F. Mauri, R. Mazzarello, S. Paolini, A. Pasquarello, L. Paulatto, C. Sbraccia, S. Scandolo, G. Sclauzero, A. P. Seitsonen, A. Smogunov, P. Umari and R. M. Wentzcovitch, *J. Phys.: Condens. Matter*, 2009, **21**, 395502.
19 F. Birch, *Phys. Rev.*, 1947, **71**, 809–824.
20 A. Dal Corso, *J. Phys.: Condens. Matter*, 2016, **28**, 075401.
21 V. I. Marchenko and G. V. Samsonov, *Phys. Metals and Metallography*, 1963, **15**, 131–132.
22 E. Bucher, K. Andres, F. J. Disalvo, J. P. Maita, A. C. Gossard, A. S. Cooper and G. W. Hull, *Phys. Rev. B*, 1975, **11**, 500.
23 P. Villars and L. L. Calvert, *Handbook of Crystallographic Data for Intermetallic Phases*, American Society for Metals, Metals Park, OH, 1985, vol. 3.
24 A. Svane, Z. Szotek, W. M. Temmerman, J. Laegsgaard and H. Winter, *J. Phys.: Condens. Matter*, 1998, **10**, 5309.
25 T. Le Bihan, A. Bombardi, M. Idiri, S. Heathman and A. Lindbaum, *J. Phys.: Condens. Matter*, 2002, **14**, 10595.
26 V. Srivastava, A. K. Bandyapadhyay, P. K. Jha and S. P. Sanyal, *J. Phys. Chem. Solids*, 2003, **64**, 907.
27 D. Varshney, N. Kaurav, P. Sharma, S. Shah and R. K. Singh, *Phys. Status Solidi B*, 2004, **241**, 3179.
28 A. Bouhemadou, R. Khenata and M. Maamache, *J. Mol. Struct. Theochem.*, 2006, **777**, 5.
29 S. Singh, R. K. Singh and A. Gour, *Cent. Eur. J. Phys.*, 2007, **5**, 576.
30 R. W. G. Wyckoff, *Crystal Structures*, 1963, **1**, 85–237.
31 J. M. Leger, *Physica B*, 1993, **190**, 84.
32 I. Vedel, M. Redon, J. Leger, J. Rossat-Mignod and O. Vogt, *J. Phys. C: Sol. State Phys.*, 2000, **19(32)**, 6297.
33 A. Iandelli, *Gazzetta Chimica Italiana*, 1955, **85**, 881–887.
34 N. N. Zhuravlev, A. A. Stepanova and M. P. Shebatinov, *Soviet Physics, Crystallography*, 1964, **9**, 95–96.
35 A. V. Golubkov, A. V. Prokof'ev and V. M. Sergeeva, *Inorganic Materials (USSR)*, 1988, **24**, 1779–1781.
36 F. Hulliger, M. Landolt, R. Schmelczer and I. Zarbach, *Sol. State Commun.*, 1975, **17**, 751–754.
37 F. Hulliger and F. Stucki, *Zeitschrift für Physik B Condensed Matter*, 1978, **31**, 391–393.
38 L. N. Vasilev, V. M. Grabov, A. V. Golubkov, A. G. Gorobets, V. S. Oskotskii, I. A. Smirnov and V. V. Tikhonov, *Physica Status Solidi A*, 1983, **80**, 237–244.
39 F. Hulliger, M. Landolt and R. Schmelczer, in *Low-Temperature Behavior of DyS, DySe, HoS and HoSe*, ed. G. J. McCarthy, H. B. Silber, J. J. Rhyne and F. M. Kalina, Springer US, Boston, MA, 1982, pp. 455–458.
40 P. Fischer, W. Hälg and F. Hulliger, *Physica B+C*, 1985, **130**, 551–554.
41 P. Fischer, W. Halg and F. Hulliger, *Physica B+C*, 1985, **130**, 551–554.
42 A. Eliseev, *Zhurnal Neorganicheskoi Khimii*, 1984, **29**, 1650–1654.
43 A. Jayaraman, P. D. Dernier and L. D. Longinotti, *Proc. Int. Conf.*, 1977, **1977**, 61–70.
44 F. Hulliger and G. Hull, *Sol. State Commun*, 1970, **8**, 1379–1382.
45 W. A. Grosshans, Y. K. Vohra and W. B. Holzapfel, *Phys. Rev. Lett.*, 1982, **49**, 1572–1575.
46 D. Errandonea, R. Boehler and M. Ross, *Phys. Rev. Lett.*, 2000, **85**, 3444–3447.
47 R. D. Shannon, *Acta Crystallographica Section A*, 1976, **32**, 751–767.
48 A. Werner, H. Hochheimer, A. Jayaraman and J. Leger, *Sol. State Commun.*, 1981, **38**, 325–327.
49 S. Akter, J. Vargas, K. Sharkas, J. Peralta, K. Jackson, T. Baruah and R. Zope, *Phys. Chem. Chem. Phys.*, 2021, **23**, 18678–18685.
50 J. Hafner, *J. Comput. Chem.*, 2008, **29**, 2044–2078.
51 Z. Chen, H. Xiao and X. Zu, *Physica B*, 2007, **391**, 193–198.
52 L. Louail, O. Krachni, A. Bouguerra and F. Ali Sahraoui, *Mat. Lett.*, 2006, **60**, 3153–3155.
53 Y. Sato and R. Jeanloz, *J. Geophys. Res.: Solid Earth*, 1981, **86**, 11773–11778.
54 K. Syassen, *Physica Status Solidi A*, 1985, **91**, 11–15.
55 S. Yamaoka, O. Shimomura, H. Nakazawa and O. Fukunaga, *Sol. State Commun.*, 1980, **33**, 87–89.
56 S. T. Weir, Y. K. Vohra and A. L. Ruoff, *Phys. Rev. B*, 1986, **33**, 4221–4226.
57 T. S. Duffy, D. J. Weidner and M. L. Rivers, *J. Phys. Chem. Sol.*, 1998, **59**, 599–603.
58 J. K. Wicks, S. Singh, M. Millot, D. E. Fratanduono, F. Coppari, M. G. Gorman, Z. Ye, J. R. Rygg, A. Hari, J. H. Eggert, T. S. Duffy and R. F. Smith, *Science Advances*, 2024, **10**, eadk0306.
59 G. Vaitheeswaran, V. Kanchana, A. Svane, N. E. Christensen, J. S. Olsen, J.-E. Jørgensen and L. Gerward, *Phys. Rev. B*, 2011, **83**, 184108.

View Article Online
DOI: 10.1039/D6DT00593D

60 M. Born and K. Huang, *Dynamical theory of crystal lattices*, Oxford university press, 1996.
61 Z.-J. Wu, E.-J. Zhao, H.-P. Xiang, X.-F. Hao, X.-J. Liu and J. Meng, *Phys. Rev. B*, 2007, **76**, 054115.
62 D. Pettifor, *Mat. Sci. Techn.*, 1992, **8**, 345–349.
63 W. Voigt, *Lehrbuch der kristallphysik:(mit ausschluss der kristalloptik)*, BG Teubner, 1910, vol. 34.
64 A. Reuß, *ZAMM-Journal of Applied Mathematics and Mechanics/Zeitschrift für Angewandte Mathematik und Mechanik*, 1929, **9**, 49–58.
65 R. Hill, *Proceedings of the Physical Society. Section A*, 1952, **65**, 349.
66 S. Pugh, *The London, Edinburgh, and Dublin Philosophical Magazine and Journal of Science*, 1954, **45**, 823–843.
67 S. K. Mishra, M. K. Gupta, R. Mittal, A. I. Kolesnikov and S. L. Chaplot, *Phys. Rev. B*, 2016, **93**, 214306.
68 S. Bag, S. Malgope, M. K. Gupta, S. K. Mishra, R. Mittal, S. Rols and S. L. Chaplot, *Phys. Rev. Mater.*, 2025, **9**, 104411.

View Article Online
DOI: 10.1039/D6DT00593D

Data availability

The data that support the findings of this article are available from the authors upon reasonable request.